



Ballistic-diffusive heat conduction in multiply-constrained nanostructures



Yu-Chao Hua, Bing-Yang Cao*

Key Laboratory for Thermal Science and Power Engineering of Ministry of Education, Department of Engineering Mechanics, Tsinghua University, Beijing 100084, China

ARTICLE INFO

Article history:

Received 17 July 2015
Received in revised form
12 October 2015
Accepted 27 October 2015
Available online xxx

Keywords:

Thermal conductivity
Nanostructures
Phonon Boltzmann transport equation
Monte Carlo simulation

ABSTRACT

Ballistic-diffusive heat conduction in multiply-constrained nanostructures is theoretically studied based on the phonon Boltzmann transport equation. The results show that different constraints influence the thermal transport in different ways. In the direction parallel to the heat flow, the phonon ballistic transport can cause temperature jumps at the boundaries in contact with the phonon baths. In contrast, for lateral constraint, the heat flux is reduced near the boundaries due to phonon-boundary scattering. A thermal conductivity model for multiply-constrained nanostructures is then derived from the phonon Boltzmann transport equation. The influences of different constraints are combined on the basis of Matthiessen's rule. The model accurately characterizes the thermal conductivities of various typical nanostructures, including nanofilms (in-plane and cross-plane) and finite length nanowires of various cross-sectional shapes (e.g. circular and rectangular). The model predictions also agree well with Monte Carlo simulations and experimental data for silicon nanofilms and nanowires.

© 2015 Elsevier Masson SAS. All rights reserved.

1. Introduction

The rapid development of nanotechnologies necessitates an in-depth understanding of nanoscale thermal transport [1]. At the macroscale, the transport in the diffusive limit corresponds to the classical Fourier's law, $q = -k\nabla T$, where q is the heat flux, T is the temperature and k represents the thermal conductivity which is an important intrinsic property of all materials. For nanomaterials in which the heat carrier mean free path (MFP) is comparable to the characteristic length, the ballistic transport and boundary scattering make the thermal conductivity dependent on the nanostructure geometry and size, indicating a violation of Fourier's law [2–11]. The presence of both diffusive and ballistic transport mechanisms leads to ballistic-diffusive heat conduction [12]. The interest in the size-dependent thermal conductivity of semiconductor nanostructures in the ballistic-diffusive regime has been growing owing to their many applications in electronics and photonics [1].

For semiconductor materials (e.g. silicon), phonons dominate the thermal transport. In the ballistic-diffusive regime, phonon

transport is characterized by the phonon Boltzmann transport equation (BTE) with a relaxation time approximation

$$v_g \cdot \nabla f = \frac{f_0 - f}{\tau}, \quad (1)$$

in which f is the phonon distribution function, f_0 is the equilibrium distribution function, v_g is the phonon group velocity and τ is the relaxation time. The influence of the boundaries is not directly seen in Eq. (1) but is seen in the imposed boundary conditions, with different boundary conditions having different influences on the thermal transport. Theoretical studies of the size-dependent thermal conductivity have been conducted especially for nanostructures with only simple boundary constraints, such as nanofilms (in-plane or cross-plane) [13–16] and nanowires with particular cross sectional shapes and infinite lengths [17–19]. Engineering systems generally have more than one constraint on the nanostructures, e.g. finite length nanowires used in experiments [20,21]. The experiments of Chen et al. [20] showed that the thermal conductivities of silicon nanowires were mainly dependent on the diameter, since the nanowires were several microns long. In contrast, the experiments of Hsiao et al. [21] demonstrated that the thermal conductivities of silicon-germanium nanowires were strongly correlated with the length but not the diameter. Although

* Corresponding author.

E-mail addresses: huayuchao19@163.com (Y.-C. Hua), caoby@tsinghua.edu.cn (B.-Y. Cao).

Alvarez and Jou [15,22] proposed a model considering multiple constraints by introducing an effective characteristic length, the influences of the different constraints on the thermal transport were not identified in their model. The size and geometry dependence of the thermal conductivity in multiply-constrained nanostructures is still poorly understood and a general characterization of their thermal conductivities is needed. Present work theoretically studies the ballistic-diffusive heat conduction in multiply-constrained nanostructures based on the phonon BTE. The influences of different constraints on the thermal transport have been clarified and a phonon thermal conductivity model is given for multiply-constrained nanostructures. The model characterizes the thermal conductivities of various typical nanostructures, including nanofilms (in-plane and cross-plane) and finite length nanowires of arbitrary cross-sectional shapes.

2. Thermal conductivity model of multiply-constrained nanostructures

Fig. 1 shows a representative geometry of multiply-constrained nanostructure. This geometry can reduce to other typical nanostructures, including nanofilms (cross-plane and in-plane) and nanowires with varied cross sections. The left and right sides are in contact with the hot (T_1) and cold (T_2) phonon baths. The heat flux, q , caused by the temperature difference is along the x -direction. The length in this direction is denoted by L_x . The lateral boundaries are adiabatic and the phonons scatter at them with a specular scattering rate p . The thermal conductivity is related to both the longitudinal length, L_x , and the size and geometry of the cross section.

The thermal conductivity of the multiply-constrained system can be calculated by solving the phonon BTE. However, an analytical solution of the phonon BTE is rather difficult to obtain when simultaneously considering all the constraints. Another way to solve this complicated problem is to deal with the constraints separately. Their effects on the thermal conductivity are then combined based on Matthiessen's rule. In the longitudinal direction (x -direction) parallel to the heat flow, the ballistic transport of the phonons can cause temperature jumps at the boundaries [23], which will reduce the thermal conductivity, while for the lateral constraint, the phonon-boundary scattering reduces the heat flux near the boundaries which reduces the thermal conductivity. Therefore, different methods should be used for different constraints.

2.1. Longitudinal constraint

First consider the longitudinal constraint. The corresponding one-dimensional BTE is,

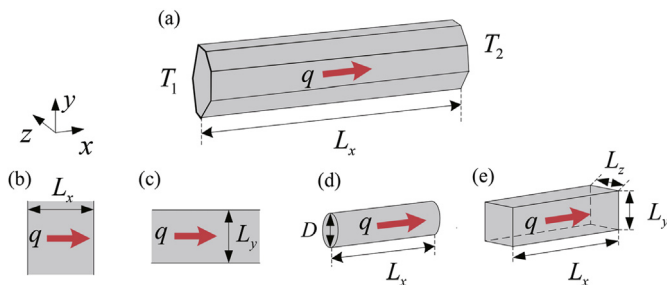


Fig. 1. Representative geometry of a multiply-constrained nanostructure (a). It can typically reduce to: (b) a nanofilm (cross-plane), (c) a nanofilm (in-plane), (d) a circular nanowire, and (e) a rectangular nanowire.

$$\mu l_0 \frac{\partial f}{\partial x} = f_0 - f, \quad (2)$$

where $\mu = \cos(\theta)$ in which θ is the polar angle between the phonon motion direction and the x -axis and l_0 is the bulk MFP equal to $v_g \tau$. For this case, Majumdar [13] proposed the gray model based on the differential approximation, but it is invalid for large Knudsen number. Here, the gray model was improved by dividing the distribution function into two parts, $f = f_b + f_d$, where f_b is the ballistic part directly originating from the boundaries and f_d is the diffusive part described by the differential approximation. This methodology was first proposed by Ofle [24] for calculating radiation heat transfer and Chen [12] then applied it to model transient ballistic-diffusive heat conduction.

The ballistic distribution function is given by,

$$\mu l_0 \frac{\partial f_b}{\partial x} = -f_b. \quad (3)$$

The ballistic heat flux, q_b , is then,

$$q_b = 2\pi \left[\int_0^1 \exp\left(-\frac{x}{\mu l_0}\right) \mu d\mu I_{w1} - \int_0^1 \exp\left(-\frac{L_x - x}{\mu l_0}\right) \mu d\mu I_{w2} \right] \quad (4)$$

with

$$I_{w1} = \varepsilon I_{01} + 2(1 - \varepsilon) \int_0^1 \exp\left(-\frac{L_x}{\mu l_0}\right) \mu d\mu I_{w2}, \quad (5)$$

$$I_{w2} = \varepsilon I_{02} + 2(1 - \varepsilon) \int_0^1 \exp\left(-\frac{L_x}{\mu l_0}\right) \mu d\mu I_{w1}, \quad (6)$$

in which ε is the phonon emissivity, $I_{01} = \int v_g \hbar \omega f_0(T_1) \text{DOS}(\omega) d\omega = \rho c_v v_g T_1 / (4\pi)$ and $I_{02} = \int v_g \hbar \omega f_0(T_2) \text{DOS}(\omega) d\omega = \rho c_v v_g T_2 / (4\pi)$ where $\text{DOS}(\omega)$ is the density of states, c_v is the volumetric specific heat and ρ is the mass density. For convenience, define the exponential integral function $E_n(t) = \int_0^1 \exp(-t/\mu) \mu^{n-2} d\mu$ and the ballistic heat flux as,

$$q_b = 2\pi \left[I_{w1} E_3\left(\frac{x}{l_0}\right) - I_{w2} E_3\left(\frac{L_x - x}{l_0}\right) \right]. \quad (7)$$

The diffusive distribution function is governed by,

$$\mu l_0 \frac{\partial f_d}{\partial x} = f_0 - f_d. \quad (8)$$

The differential approximation of Eq. (8) yields

$$q_d = q - q_b = \frac{1}{3} \rho c_v v_g l_0 \frac{\partial T_d}{\partial x}, \quad (9)$$

with the Marshak boundary conditions [25].

$$T_d(0) - \frac{4l_0}{3} \left(\frac{1}{\varepsilon} - \frac{1}{2} \right) \frac{\partial T_d(0)}{\partial x} = 0, \quad (10)$$

$$T_d(L_x) + \frac{4l_0}{3} \left(\frac{1}{\varepsilon} - \frac{1}{2} \right) \frac{\partial T_d(L_x)}{\partial x} = 0, \quad (11)$$

in which q_d is the diffusive heat flux and T_d is defined as $T_d = \frac{2\pi}{\rho c_v v_g} \int_{-1}^1 d\mu \int \hbar \omega v_g f_d \text{DOS}(\omega) d\omega$. The boundary conditions

chosen for the diffusive component are called the Marshak boundary conditions, which have been widely adopted in the heat radiation and neutron transport [25]. Since the boundary does not contribute to the diffusive component, the diffusive heat flux at the boundary is only made of the incident diffusive carriers. Then, the Marshak boundary condition can be deduced by the differential approximation [25]. The similar boundary conditions were used in Ofle's work [24] where a heat radiation problem was solved by the splitting method. These boundary conditions characterize the boundary temperature jump caused by the ballistic transport.

The effective temperature, $T(x)$, which is a representation of the average energy of all phonons around a local point, is defined as $T(x) = \frac{2\pi}{\rho c_v v_g} \int_{-1}^1 d\mu \int \hbar \omega v_{gf}(x) \text{DOS}(\omega) d\omega$. These equations are combined with the energy conservation equation, $\partial q / \partial x = 0$, to give the temperature profile,

$$T(x) = \frac{2 \left[q_b(0) - q \right] - \frac{3q}{l_0} x + \frac{3}{l_0} \int_0^x q_b dx + 2\pi \left[I_{w1} E_2 \left(\frac{x}{l_0} \right) - I_{w2} E_2 \left(\frac{L_x - x}{l_0} \right) \right]}{\rho c_v v_g}, \quad (12)$$

in which the heat flux, q , is

$$q = \frac{\rho v_g c_v l_0 (T_1 - T_2)}{3L_x} \frac{\frac{1}{\varepsilon} + \left(\frac{2}{\varepsilon} - 1 \right) E_3 \left(\frac{L_x}{l_0} \right) - \frac{3}{2} E_4 \left(\frac{L_x}{l_0} \right)}{\left(1 + \frac{4l_0}{3L_x} \left(\frac{2}{\varepsilon} - 1 \right) \right) \left(\frac{1}{\varepsilon} + 2 \left(\frac{1}{\varepsilon} - 1 \right) E_3 \left(\frac{L_x}{l_0} \right) \right)}. \quad (13)$$

Using Fourier's law, the longitudinal constrained thermal conductivity is,

$$k_x = \frac{k_{bulk}}{F}, \quad (14)$$

where $k_{bulk} = \rho c_v v_g l_0 / 3$ and F is

$$F = \frac{\left(1 + \frac{4l_0}{3L_x} \left(\frac{2}{\varepsilon} - 1 \right) \right) \left(\frac{1}{\varepsilon} + 2 \left(\frac{1}{\varepsilon} - 1 \right) E_3 \left(\frac{L_x}{l_0} \right) \right)}{\frac{1}{\varepsilon} + \left(\frac{2}{\varepsilon} - 1 \right) E_3 \left(\frac{L_x}{l_0} \right) - \frac{3}{2} E_4 \left(\frac{L_x}{l_0} \right)}. \quad (15)$$

Eq. (14) can be rewritten into the form of Matthiessen's rule as $k_x / k_{bulk} = (1 + l_0 / l_x)^{-1}$. The longitudinal constrained MFP, l_x , is

$$l_x = \frac{l_0}{F - 1}. \quad (16)$$

2.2. Lateral constraint

The corresponding phonon BTE for the lateral constraint [17] is,

$$v_{gx} \frac{\partial f_0}{\partial T} \frac{\partial T}{\partial x} + v_{gy} \frac{\partial f_1}{\partial y} + v_{gz} \frac{\partial f_1}{\partial z} = -\frac{f_1}{\tau}, \quad (17)$$

where $f_1 = f - f_0$. In Eq. (17), the influence of longitudinal constraint is neglected, so $\partial f_1 / \partial x$ vanishes. Moreover, there is no temperature gradient in the y - and z -directions. Eq. (17) can be solved using the methodology developed to calculate the size-dependent electrical conductivity [2]. Phonon scattering at the boundaries with specular scattering rate p corresponds to the boundary condition [2], $f_1(y_B, z_B)_{v_n} = p f_1(y_B, z_B)_{-v_n}$, where the planar vector $r_B(y_B, z_B)$ describes the lateral boundary profile. Thus, Eq. (17) has the following

solution

$$f_1 = v_{gx} \tau \frac{\partial f_0}{\partial T} \frac{\partial T}{\partial x} \left[\frac{(1-p) \exp \left(-\frac{\sqrt{(y-y_B)^2 + (z-z_B)^2}}{\sqrt{v_{gy}^2 + v_{gz}^2} \tau} \right)}{1 - p \exp \left(-\frac{\sqrt{(y-y_B)^2 + (z-z_B)^2}}{\sqrt{v_{gy}^2 + v_{gz}^2} \tau} \right)} - 1 \right]. \quad (18)$$

The heat flux along the x -direction can be calculated as,

$$q_x(y, z) = \int \text{DOS}(\omega) d\omega \int_{-1}^1 \int_0^{2\pi} v_g \omega \hbar f_1 \mu d\mu d\varphi, \quad (19)$$

in which φ is the azimuth angle. According to Eq. (18), the heat flux q_x decreases near the boundaries due to the phonon-boundary scattering. The heat flow can be calculated as $Q_x = \int q_x(y, z) dS$, where S is the cross sectional area. Using Fourier's law, the thermal conductivity is then,

$$k_c = \frac{k_{bulk}}{G}, \quad (20)$$

with

$$G^{-1} = 1 - \frac{3}{4\pi S} \int_S dS \int_{-1}^1 \int_0^{2\pi} \frac{(1-p) \exp \left(-\frac{\sqrt{(y-y_B)^2 + (z-z_B)^2}}{l_0 \sqrt{1-\mu^2}} \right)}{1 - p \exp \left(-\frac{\sqrt{(y-y_B)^2 + (z-z_B)^2}}{l_0 \sqrt{1-\mu^2}} \right)} \mu^2 d\mu d\varphi. \quad (21)$$

Eq. (20) can also be rewritten into the form of Matthiessen's rule as $k_c/k_{bulk} = (1 + l_0/l_c)^{-1}$ with the lateral constrained MFP, l_c , as

$$l_c = \frac{l_0}{G - 1}. \quad (22)$$

2.3. Combination of different constraint influences

The confined MFP resulting from the longitudinal and lateral constraints can be obtained based on Matthiessen's rule,

$$l_t = \frac{1}{l_0^{-1} + l_x^{-1} + l_c^{-1}}. \quad (23)$$

The system thermal conductivity shown in Fig. 1 is calculated as $k_{eff} = \rho c_v v_{gl} l_t / 3$, in which the mass density, the specific heat and the group velocity are assumed to be the same as in the bulk material [26]. Hence, the ratio of the size-dependent thermal conductivity to the bulk value is,

$$\frac{k_{eff}}{k_{bulk}} = \frac{l_t}{l_0} = \frac{1}{1 + l_0/l_x + l_0/l_c}. \quad (24)$$

A thermal conductivity model in the form of Eq. (24) is,

$$\frac{k_{eff}}{k_{bulk}} = \frac{1}{F + G - 1}, \quad (25)$$

where G is a general term related to the arbitrary cross sectional shape. The expressions of G for the lateral constraints in nanofilms and in circular and rectangular nanowires with diffusively scattering lateral boundaries ($p = 0$) are [2,17,27],

$$G_{inp}^{-1} = 1 - \frac{3l_0}{2L_y} \int_0^1 \left(1 - \exp\left(-\frac{L_y}{\sqrt{1-\mu^2}l_0}\right) \right) \mu^3 d\mu; \quad (26)$$

$$G_{cir}^{-1} = 1 - \frac{12}{\pi D^2} \int_0^{D/2} r dr \int_0^{2\pi} \int_0^1 \exp\left(-\frac{D \sin\left(\varphi - \arcsin\left(\frac{2r}{D} \sin(\varphi)\right)\right)}{2 \sin(\varphi) \sqrt{1-\mu^2} l_0}\right) \mu^2 d\mu d\varphi; \quad (27)$$

$$G_{rec}^{-1} = 1 - \frac{3}{\pi L_y L_z} \int_0^{L_y} dy \int_0^{L_z} dz \int_0^1 \left[\int_{\phi_1}^{\phi_2} \exp\left(-\frac{L_y - y}{\sin(\varphi) \sqrt{1-\mu^2} l_0}\right) d\varphi + \int_{\phi_2}^{\phi_3} \exp\left(\frac{z}{\cos(\varphi) \sqrt{1-\mu^2} l_0}\right) d\varphi \right] \mu^2 d\mu, \quad (28)$$

where L_y in Eq. (26) is the nanofilm thickness, D in Eq. (27) is the circular nanowire diameter, L_z and L_y in Eq. (28) are the width and height of a rectangular nanowire, $\phi_1 = \arctan[(L_y - y)/(L_z - z)]$, $\phi_2 = \pi/2 + \arctan[z/(L_y - y)]$, and $\phi_3 = \pi + \arctan(y/z)$. Substituting G_{inp} into Eq. (25) yields a thermal conductivity model for

nanofilms with finite length and thickness, while combining G_{cir} and G_{rec} with Eq. (25) leads to the models for finite length circular and rectangular nanowires.

This model can be easily extended to take the phonon dispersion into account. When considering the size-dependence of the thermal conductivity at room temperature, the contribution of momentum-conserving collisions (normal scattering) can be assumed to be negligible, especially for semiconductors [11]. Therefore the standard relaxation time approximation model [28–31] can be used,

$$k_{eff} = \frac{1}{3} \sum_j \int_0^{\omega_{mj}} \hbar \omega \frac{\partial f_0(\omega, T)}{\partial T} v_{gj}(\omega) l_{tj}(\omega, T) DOS_j(\omega) d\omega, \quad (29)$$

with $l_{tj}(\omega, T) = l_{0j}(\omega, T) / [F(l_{0j}) + G(l_{0j}) - 1]$, in which l_{0j} is the intrinsic phonon MFP of frequency ω and polarization j , and the modified MFP, l_{tj} , reflects the influence of the multiple constraints.

3. Model verification

A Monte Carlo (MC) technique [23,32] was used to directly solve the phonon BTE. The MC technique is a well-developed tool for phonon heat conduction simulations. It simulates phonon transport processes by random number samplings, equivalent to directly solving the phonon BTE. In the MC simulations, phonons start from the heat sinks and are traced in the domains until they exit through the x -directional boundaries. The intrinsic scattering processes, such as phonon-impurities and phonon-phonon scatterings, are treated in the relaxation-time approximation. The Knudsen numbers were defined as $Kn_x = l_0/L_x$, $Kn_y = l_0/L_y$, $Kn_z = l_0/L_z$ and $Kn_D = l_0/D$.

Fig. 2 compares the heat flux distributions and temperature profiles obtained from the analytical solutions and the MC simulations. The results in Fig. 2 (a) considered only the longitudinal constraint and the phonon emissivity ε was set to 1.0. Eq. (12) was used to characterize the temperature profiles. The boundary temperature jumps due to the ballistic transport increase as Kn_x increases [23]. The predictions of Eq. (12) agree well with the MC simulations. Fig. 2 (b) compares the heat flux distributions in

nanofilms (in-plane) predicted by the analytical solution and the MC simulations. The specular scattering rate, p , was set to 0.0. Eq. (19) can characterize the heat flux distributions in nanofilms (in-plane). The heat flux is reduced near boundaries owing to phonon-boundary scattering, so the heat flux decreases with increasing Kn_y .

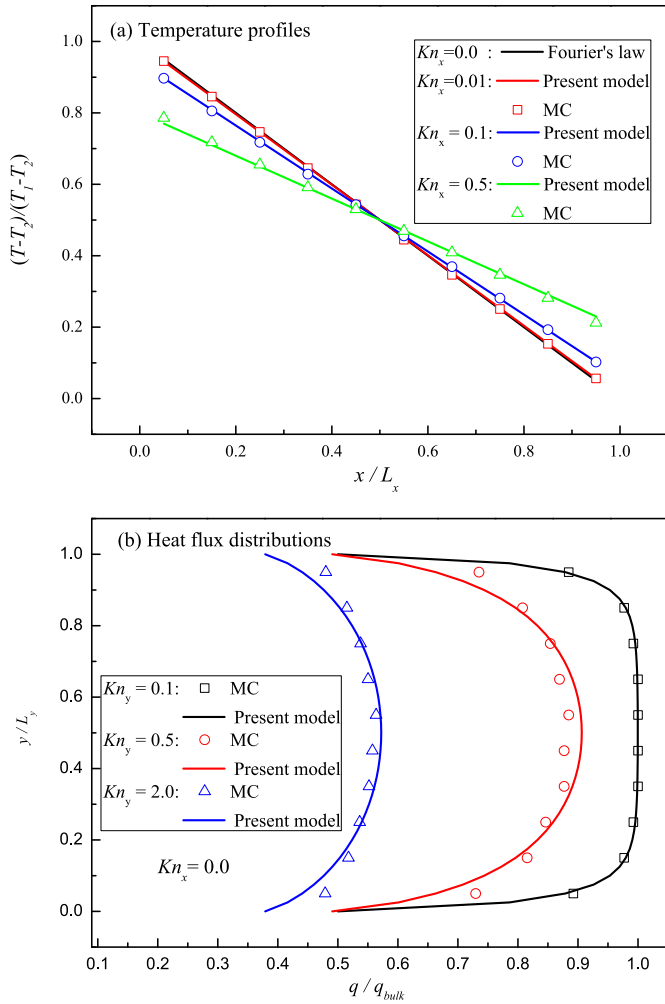


Fig. 2. Comparison of the analytical solutions with MC simulations: (a) temperature profiles, (b) heat flux distributions.

Eq. (19) accurately predicts the heat flux distributions predicted by the MC simulations.

Fig. 3 compares the thermal conductivities predicted by the models and the Monte Carlo simulations. The model by Alvarez and Jou [22] is also given for comparison. The nanofilm thermal conductivities are illustrated in Fig. 3(a). For a given Kn_x , the thermal conductivity decreases with increasing Kn_y and vice versa. The present model agree better with the MC simulations than Alvarez and Jou's model [22], because the effective characteristic length in Alvarez and Jou's model assumes that the constraints have the same effect regardless of their different influences on the thermal conductivity. Although in some cases Alvarez and Jou's model can slightly deviate from the MC simulations, it is also helpful and convenient in the practical applications due to its straightforward physical meaning and simple expression. Fig. 3 (b) and (c) show the thermal conductivities of circular and square nanowires. The thermal conductivity size-dependent behavior for the finite length circular and square nanowires is the same as for the nanofilms. The agreement between the MC simulations and present model indicates the validity of this model.

The predictions of the present model are compared with available experimental data for silicon nanostructures [3–9] at room temperature in Fig. 4. The experimental data was converted to dimensionless units using a bulk thermal conductivity of 150 W/m-

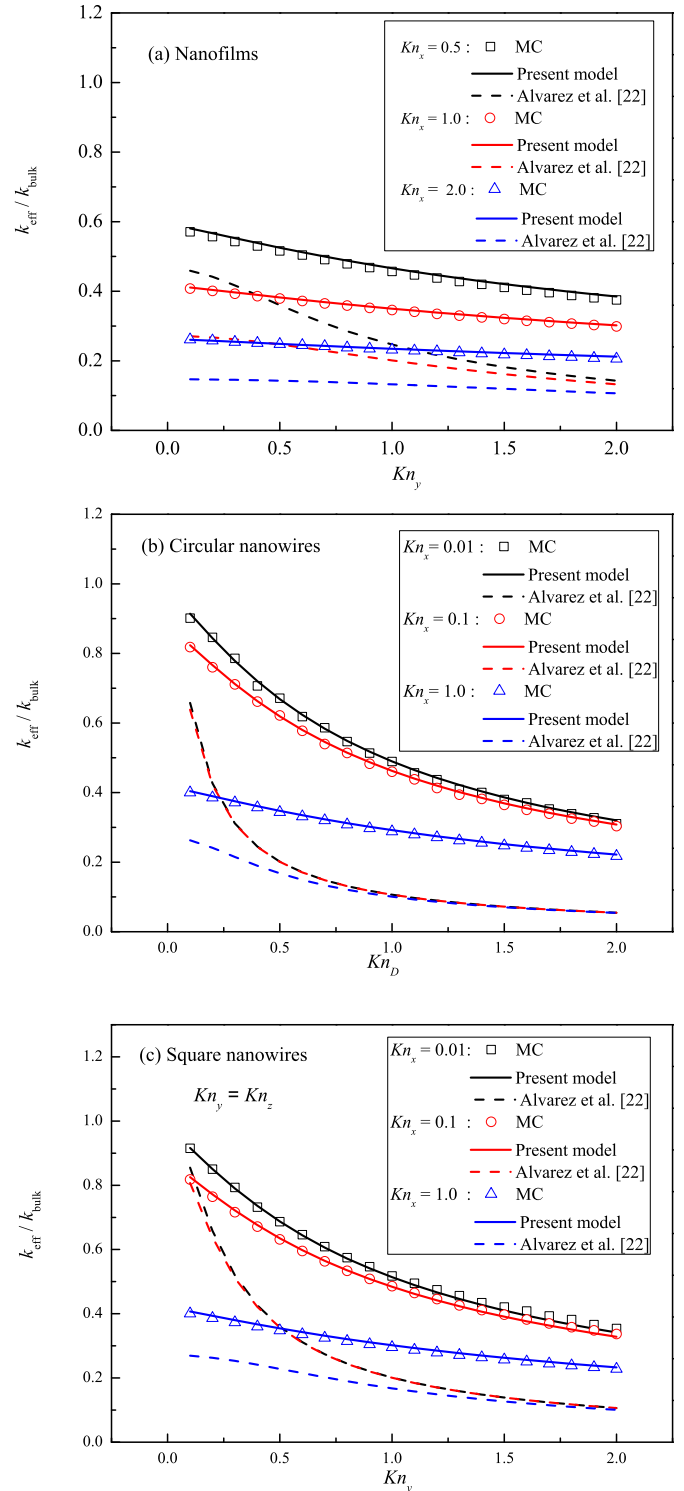


Fig. 3. Thermal conductivities predicted by the current models and the Monte Carlo simulations: (a) nanofilms, (b) circular nanowires, (c) square nanowires.

K and a MFP for bulk silicon of 210 nm according to references [33,26] where the value of bulk silicon MFP at room temperature varied between 200 nm and 300 nm. It should be noted that arguments still exist for the phonon MFP of silicon at room temperature. When considering both the acoustic and optical phonons, the MFP is about 43.7 nm [23], while only considering acoustic phonons that carry most of heat, it becomes much longer [26]. In fact,

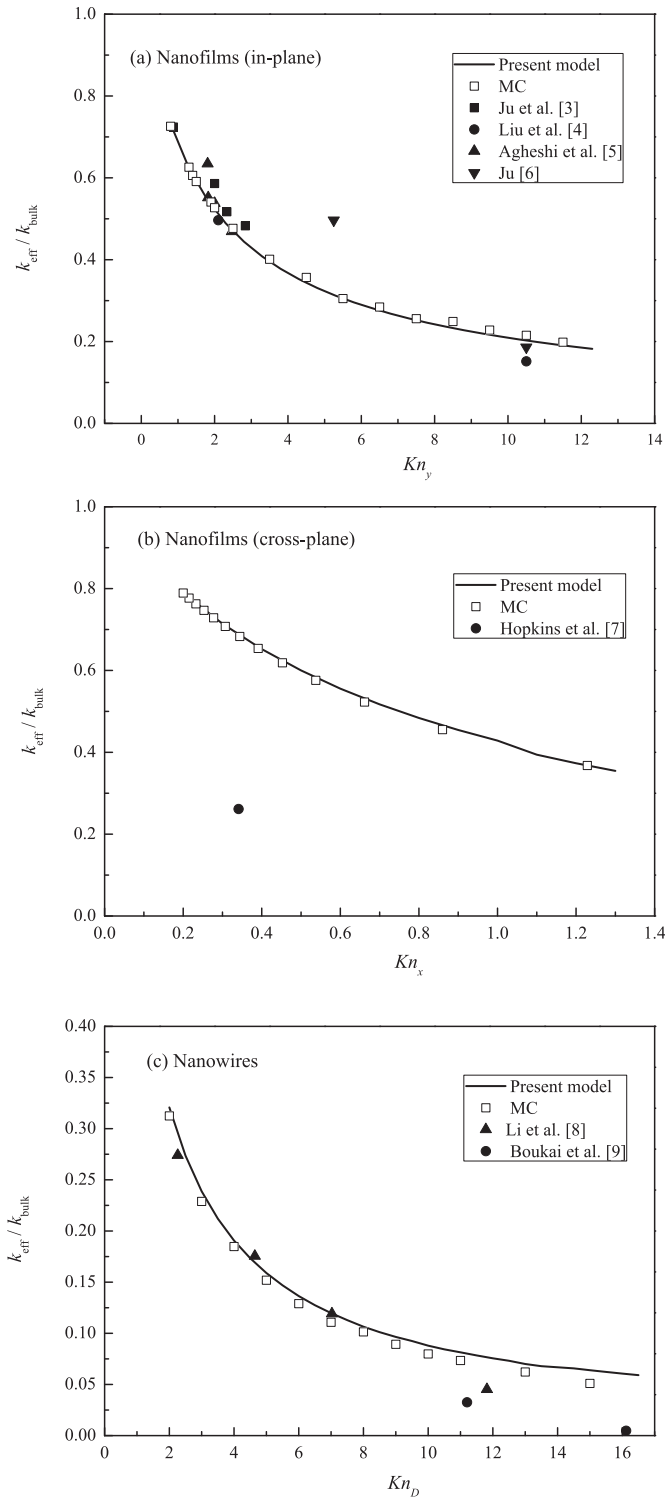


Fig. 4. Comparison of the thermal conductivities predicted by the present model with experimental data for silicon nanostructures [3–9]: (a) nanofilms (in-plane), (b) nanofilms (cross-plane), (c) nanowires.

since all the quantities in the MC simulations and the models are dimensionless in Figs. 2 and 3, the choice of the MFP does not influence the comparisons between them. However, when compared with the experimental data in Fig. 4, it was found that the longer phonon MFP is the better choice to characterize the size dependent behavior of the thermal conductivity [3,26]. When the x -directional

Knudsen number, Kn_x , is equal to 0, the present model gives the in-plane thermal conductivity of a nanofilm. The results in Fig. 4(a) show that the predictions of the present model agree well with the experimental data and the MC simulations. The slight difference between the model and experimental data may result from the choice of the phonon MFP. When the y -directional Knudsen number, Kn_y , vanishes, the present model gives the cross-plane thermal conductivity of the nanofilm. The data in Fig. 4(b) shows that the model also agree well with the MC simulations, but the experimental data from Hopkins et al. [7] is much lower than the model predictions. A similar result was also reported by McGaughey et al. [34]. For long nanowires in which the contribution of the longitudinal (x -direction) constraint can be neglected, the x -directional Knudsen number, Kn_x , is equal to 0. The data in Fig. 4(c) shows that the present model predictions agree well with the MC simulations. Moreover, the model and the experimental data are also consistent, for Kn_D less than 10. For Kn_D larger than 10, the model over-predicts the experimental data. Changes in the phonon dispersion will further reduce of the thermal conductivity [35,36] for nanowire diameters much smaller than the bulk phonon MFP ($Kn_D > 10.0$).

4. Conclusions

Analyses of the ballistic-diffusive heat conduction in multiply-constrained nanostructures showed that different constraints lead to different effects on the thermal transport. Phonon ballistic transport in the heat flow direction can cause temperature jumps at the boundaries in contact with the phonon baths. The phonon-boundary scattering due to the lateral constraint will reduce the heat flux near the boundaries.

An analytical model was derived for the phonon thermal conductivity of multiply-constrained nanostructures from the phonon BTE with the constraints analyzed separately. A modified differential approximation method was used for the longitudinal constraint in the heat flow direction, while the lateral constraint was characterized by directly solving the phonon BTE. Then, the effects of the different constraints on thermal conductivity are combined based on Matthiessen's rule. This model can accurately predict the thermal conductivities of various nanostructures, including nanofilms (in-plane and cross-plane) and finite length nanowires of arbitrary cross-sectional shapes. The model predictions for finite length and finite thickness nanofilms and finite length circular and square nanowires are coincident with the MC simulations. The model predictions also agree well with experimental data for silicon nanofilms and nanowires. It should be noted that the Matthiessen's rule assumes that the different scattering progresses are independent. However, this assumption cannot always be valid [37]. We have combined the multiply phonon-boundary scattering effects via the Matthiessen's rule, ignoring the coupling effect. The present model's good agreements with the MC simulations and the experimental data have demonstrated that the coupling effect between phonon-boundary scatterings is not significant for the relatively simple multiply-constrained nanostructures, such as nanofilms and finite length nanowires. As for more complex multiply-constrained nanostructures, the present methodology should be improved to take the coupling effect into account.

Acknowledgments

This work was financially supported by the National Natural Science Foundation of China (Nos. 51322603, 51136001, and 51356001), the Science Fund for Creative Research Group (No. 51321002), and the Tsinghua National Laboratory for Information Science and Technology of China (TNList).

References

- [1] E.S. Toberer, L.L. Baranowski, C. Dames, *Advances in thermal conductivity*, *Annu. Rev. Mater. Res.* 42 (2012) 179–209.
- [2] J.M. Ziman, *Electrons and Phonons: the Theory of Transport Phenomena in Solids*, Clarendon Press Oxford, UK, 2001.
- [3] Y. Ju, K.E. Goodson, Phonon scattering in silicon films with thickness of order 100 nm, *Appl. Phys. Lett.* 74 (20) (1999) 3005–3007.
- [4] W. Liu, M. Asheghi, Phonon–boundary scattering in ultrathin single-crystal silicon layers, *Appl. Phys. Lett.* 84 (19) (2004) 3819–3821.
- [5] M. Asheghi, Y. Leung, S. Wong, K. Goodson, Phonon-boundary scattering in thin silicon layers, *Appl. Phys. Lett.* 71 (13) (1997) 1798–1800.
- [6] Y. Ju, Phonon heat transport in silicon nanostructures, *Appl. Phys. Lett.* 87 (15) (2005) 153106.
- [7] P.E. Hopkins, C.M. Reinke, M.F. Su, R.H. Olsson III, E.A. Shaner, Z.C. Leseman, J.R. Serrano, L.M. Phinney, I. El-Kady, Reduction in the thermal conductivity of single crystalline silicon by phononic crystal patterning, *Nano Lett.* 11 (1) (2010) 107–112.
- [8] D. Li, Y. Wu, P. Kim, L. Shi, P. Yang, A. Majumdar, Thermal conductivity of individual silicon nanowires, *Appl. Phys. Lett.* 83 (14) (2003) 2934–2936.
- [9] A.I. Boukai, Y. Bunimovich, J. Tahir-Kheli, J.-K. Yu, W.A. Goddard III, J.R. Heath, Silicon nanowires as efficient thermoelectric materials, *Nature* 451 (7175) (2008) 168–171.
- [10] M. Szymański, Calculation of the cross-plane thermal conductivity of a quantum cascade laser active region, *J. Phys. D Appl. Phys.* 44 (8) (2011) 085101.
- [11] T. Feng, X. Ruan, Prediction of spectral phonon mean free path and thermal conductivity with applications to thermoelectrics and thermal management: a review, *J. Nanomater* 2014 (2014) 206370.
- [12] G. Chen, Ballistic-diffusive heat-conduction equations, *Phys. Rev. Lett.* 86 (11) (2001) 2297.
- [13] A. Majumdar, Microscale heat conduction in dielectric thin films, *J. Heat. Trans.* 115 (1) (1993) 7–16.
- [14] G. Chen, C. Tien, Thermal conductivities of quantum well structures, *J. Thermophys. Heat. Tr.* 7 (2) (1993) 311–318.
- [15] F. Alvarez, D. Jou, Memory and nonlocal effects in heat transport: from diffusive to ballistic regimes, *Appl. Phys. Lett.* 90 (8) (2007) 083109.
- [16] Y. Dong, B.Y. Cao, Z.Y. Guo, Ballistic–diffusive phonon transport and size induced anisotropy of thermal conductivity of silicon nanofilms, *Phys. E* 66 (2015) 1–6.
- [17] X. Lü, W. Shen, J. Chu, Size effect on the thermal conductivity of nanowires, *J. Appl. Phys.* 91 (3) (2002) 1542–1552.
- [18] A. Sellitto, F. Alvarez, D. Jou, Geometrical dependence of thermal conductivity in elliptical and rectangular nanowires, *Int. J. Heat. Mass Trans* 55 (11) (2012) 3114–3120.
- [19] Y. Dong, B.Y. Cao, Z.Y. Guo, Size dependent thermal conductivity of Si nano-systems based on phonon gas dynamics, *Phys. E* 56 (2014) 256–262.
- [20] R. Chen, A.I. Hochbaum, P. Murphy, J. Moore, P. Yang, A. Majumdar, Thermal conductance of thin silicon nanowires, *Phys. Rev. Lett.* 101 (10) (2008) 105501.
- [21] T.-K. Hsiao, H.-K. Chang, S.-C. Liou, M.-W. Chu, S.-C. Lee, C.-W. Chang, Observation of room-temperature ballistic thermal conduction persisting over 8.3 μm in SiGe nanowires, *Nat. Nanotech* 8 (7) (2013) 534–538.
- [22] F. Alvarez, D. Jou, Size and frequency dependence of effective thermal conductivity in nanosystems, *J. Appl. Phys.* 103 (9) (2008) 094321.
- [23] Y.C. Hua, B.Y. Cao, Phonon ballistic-diffusive heat conduction in silicon nanofilms by Monte Carlo simulations, *Int. J. Heat. Mass Trans* 78 (2014) 755–759.
- [24] D. Olfe, A modification of the differential approximation for radiative transfer, *AIAA J.* 5 (4) (1967) 638–643.
- [25] G. Chen, Ballistic-diffusive equations for transient heat conduction from nano to macroscales, *J. Heat. Trans.* 124 (2) (2002) 320–328.
- [26] G. Chen, Thermal conductivity and ballistic-phonon transport in the cross-plane direction of superlattices, *Phys. Rev. B* 57 (23) (1998) 14958.
- [27] R. Chambers, The conductivity of thin wires in a magnetic field, in: *P. Roy. Soc. Lond A Mat.*, vol. 202, 1950, pp. 378–394.
- [28] N. Mingo, Calculation of Si nanowire thermal conductivity using complete phonon dispersion relations, *Phys. Rev. B* 68 (11) (2003) 113308.
- [29] C. De Tomas, A. Cantarero, A.F. Lopeandia, F.X. Alvarez, Thermal conductivity of group-iv semiconductors from a kinetic-collective model, *Proc. R. Soc. A Math. Phys. Eng. Sci.* 470 (2014) 2169.
- [30] C. De Tomas, A. Cantarero, A. Lopeandia, F. Alvarez, From kinetic to collective behavior in thermal transport on semiconductors and semiconductor nanostructures, *J. Appl. Phys.* 115 (16) (2014) 164314.
- [31] D.A. Broido, M. Malorny, G. Birner, N. Mingo, D.A. Stewart, Intrinsic lattice thermal conductivity of semiconductors from first principles, *Appl. Phys. Lett.* 91 (2007) 231922.
- [32] J.-P.M. Péraud, N.G. Hadjiconstantinou, An alternative approach to efficient simulation of micro/nanoscale phonon transport, *Appl. Phys. Lett.* 101 (15) (2012) 153114.
- [33] E. Pop, S. Sinha, K.E. Goodson, Heat generation and transport in nanometer-scale transistors, *Proc. IEEE* 94 (8) (2006) 1587–1601.
- [34] A.J. McGaughey, E.S. Landry, D.P. Sellan, C.H. Amon, Size-dependent model for thin film and nanowire thermal conductivity, *Appl. Phys. Lett.* 99 (13) (2011) 131904.
- [35] A. Balandin, K.L. Wang, Significant decrease of the lattice thermal conductivity due to phonon confinement in a free-standing semiconductor quantum well, *Phys. Rev. B* 58 (3) (1998) 1544.
- [36] X. Wang, B. Huang, Computational study of in-plane phonon transport in si thin films, *Sci. Rep.* 4 (2014) 6399.
- [37] J. Glasbrenner, B. Pujari, K. Belashchenko, Deviations from Matthiessen's rule and resistivity saturation effects in Gd and Fe from first principles, *Phys. Rev. B* 89 (17) (2014) 174408.